Brain Structure and Function (2022) 227:1317–1330
https://doi.org/10.1007/s00429-021-02440-3

ORIGINAL ARTICLE

Function-specific projections from V2 to V4 in macaques

Chen Fang[1] · Kun Yan[1] · Chen Liang[1] · Jiayu Wang[1] · Xingya Cai[1] · Rui Zhang[1] · Haidong D. Lu[1]

Received: 12 March 2021 / Accepted: 8 December 2021 / Published online: 3 January 2022

Abstract

Previous studies have revealed modular projections from area V2 to area V4 in macaques. Specifically, V2 neurons in cytochrome oxidase (CO)-rich thin and CO-sparse pale stripes project to distinct regions in V4. However, how these modular projections relate to the functional subcompartments of V4 remains unclear. In this study, we injected retrograde fluorescent tracers into V4 regions with different functional properties (color, orientation, and direction) that were identified with intrinsic signal optical imaging (ISOI). We examined the labeled neurons in area V2 and their locations with respect to the CO patterns. Covariation was observed between the functional properties of the V4 injection sites and the numbers of labeled neurons in particular CO stripes. This covariation indicates that the color domains in V4 mainly received inputs from thin stripes in V2, whereas V4 orientation domains received inputs from pale stripes. Although motion-sensitive domains are present in both V2 and V4, our results did not reveal a functional specific feedforward projection between them. These results confirmed previous findings of modular projections from V2 to V4 and provided functional specificity for these anatomical projections. Together, these findings indicate that color and form remain separate in ventral mid-level visual processing.

Keywords Optical imaging · Retrograde tracing · V4 · V2 · Functional architecture

Introduction

Area V2 in primates contains functionally distinct subcompartments that have been revealed with CO staining. Thin CO stripes contain more color-sensitive neurons, thick and pale stripes contain more orientation neurons, and thick stripes contain more binocular disparity and direction neurons (De Yoe and Van Essen 1985; Hubel and Livingstone 1985, 1987; Peterhans and von der Heydt 1993; Levitt et al. 1994; Shipp and Zeki 2002; Peres et al. 2018). Functional imaging also confirmed this functional segregation in V2 (Ts'o et al. 1990, 2001; Roe and Ts'o 1995; Xiao et al. 2003; Wang et al. 2007; Chen et al. 2008; Lu et al. 2010). These CO stripes also exhibit different patterns of projections to downstream areas. Neurons in thin and pale stripes mainly project to area V4, whereas neurons in thick stripes mainly project to area MT (DeYoe and Van Essen 1985; Shipp and Zeki 1985; Nascimento-Silva et al. 2003). In V2–V4 feedforward projections, thin and pale stripes appear to project to separate regions in V4 (Zeki and Shipp 1989; Nakamura et al. 1993; DeYoe et al. 1994; Felleman et al. 1997; Xiao et al. 1999), indicating a modular organization of V4 and modular connections with V2 functional organizations. However, the functional properties of these V2-receiving modules remain unclear. With the discovery of different types of functional modules in V4 (Ghose and Ts'o 1997; Conway et al. 2007; Tanigawa et al. 2010), an important goal is to establish the relationship between the anatomical and functional modules in V4. This relationship will help us to determine whether different visual features are processed in parallel or in a merged manner in the ventral visual pathway.

Area V4 is an important visual area that performs midlevel visual processing (Roe et al. 2012; Pasupathy et al. 2020). Similar to its upstream areas, V4 also contains functional modules that preferentially process color and form information (Ghose and Ts'o 1997; Conway et al. 2007; Tanigawa et al. 2010). These spatially segregated modules may receive inputs from the corresponding color and form modules in V2. One of the purposes of this study was to

Chen Fang and Kun Yan contributed equally.

✉ Haidong D. Lu
haidong@bnu.edu.cn
https://lulab.bnu.edu.cn

[1] State Key Laboratory of Cognitive Neuroscience and Learning, IDG/McGovern Institute for Brain Research, Beijing Normal University, No. 19 Xin Jie Kou Wai Street, Beijing 100875, China

provide direct evidence supporting these functional connections between V2 and V4. Motion-sensitive modules were another potential functional connection between these two areas we wanted to investigate. In both V2 (Lu et al. 2010) and V4 (Li et al. 2013), direction-selective neurons tend to cluster and form functional modules. These findings inspired us to investigate the functional link between these two modules.

In this study, we first mapped three functional responses (color, orientation, and direction) in V4 with ISOI. We then injected retrograde tracers into different V4 regions with different functional properties. Finally, we counted labeled neurons in different CO compartments in V2. We observed covariations between the labeled neurons in V2 and the functional properties of the tracer injection sites in V4; we then used this information to estimate the connections between V2 and V4 functional compartments.

Materials and methods

Animal subjects

Four adult male macaques (3 *Macaca mulatta* and 1 *Macaca fascicularis*) were examined. All procedures were performed in accordance with the National Institutes of Health Guidelines and were approved by the Institutional Animal Care and Use Committee of Beijing Normal University.

Surgery

Aseptic surgical procedures were similar to those described in a previous study (Li et al. 2013). Animals were artificially ventilated and anesthetized with isoflurane (1.5–3%) in oxygen. Heart rate, end-tidal CO_2, blood oximetry, and body temperature were closely monitored, and the anesthesia depth was estimated based on these values. A circular craniotomy (24 mm in diameter) was performed over area V4. The center of the craniotomy was 30–38 mm from the midline and 10–18 mm from the posterior bone ridge. A durotomy was performed to expose parts of areas V1, V2 and V4 (illustrated in Fig. 1a, b).

Intrinsic signal optical imaging (ISOI)

ISOI was performed immediately after surgery. The imaging procedures used in the present study were described in detail in a published article (Li et al. 2013). The brain was stabilized with a cover glass (2–3 mm thickness) and agar (4%). The anesthetic was switched to propofol (induction: 5 mg/kg, maintenance: 5 mg/kg/h, i.v.). Animals were paralyzed with vecuronium bromide (induction: 0.25 mg/kg, maintenance: 0.05 mg/kg/h, i.v.) and respirated to prevent eye movements. Atropine sulfate (10 mg/ml) or tropicamide (5 mg/ml) was applied to dilate the pupils. Appropriate contact lenses were determined using retinoscopy and used to focus the eyes on a CRT screen 57 cm from the eyes. The cortex was illuminated with 632 nm light, and the reflectance light was collected using Imager 3001 (Optical Imaging Inc., Germantown, NY) at a 4 Hz frame rate. The frame size was 654 × 540 pixels, with a pixel size of 38 μm. Each imaging session started 0.5 s before the presentation of the visual stimulus and lasted for 4 s (16 frames). The duration of the visual stimulation was 3.5 s. The intertrial interval was 8 s.

Visual stimulus

The visual stimuli used in this study were the same as those previously used to obtain functional maps (Lu et al. 2010 for V2 maps; Li et al. 2013 for V4 maps). Visual stimuli were created using ViSaGe (Cambridge Research Systems Ltd) and displayed on a 21-inch CRT monitor refreshing at 100 Hz. The stimulus patch was a full screen (30 × 40°) presented binocularly that fully covered the visual field of the imaged cortices. Two sets of gratings were used to obtain three types of functional maps (color, orientation, and direction). For the color functional map, responses to red–green isoluminant sine wave gratings and black–white sine wave gratings were compared. The spatial frequency (SF) of the gratings was 1 cycle/degree, and the temporal frequency (TF) of the gratings was 4 cycles/second. Gratings were presented in one of two orientations (45° or 135°) and in random directions orthogonal to the grating orientation. Data from different orientations were pooled. For orientation and direction maps, black–white square wave gratings were used. Gratings had an SF of 1 cycle/degree, a TF of 4 cycles/second and drifted in one of eight equally spaced directions (0°, 45°, 90°, 135°, 180°, 225°, 270°, or 315°). All stimuli were presented in a random order. An orientation map was obtained by comparing responses to orthogonal gratings (direction pooled), and a direction map was obtained by comparing responses to oppositely moving gratings.

Map-guided tracer injection

V4 injection sites were selected from the 3 functional maps (color, orientation, and direction) with the aim of maximizing differences in the responses. For monkeys A, B, and D, the cortex was stabilized with a cover glass over holes in the injection regions and a silicon membrane (~ 0.2 mm) underneath. For monkey C, the cortex was stabilized with a cover glass and agar. Three types of retrograde tracers (CTB-488, CRB-555, and CTB-647; 1%, Invitrogen) were used in this study. A pressure injection system (53,311, Stoelting) and a glass pipette with a tip size of 23–35 μm (beveled)

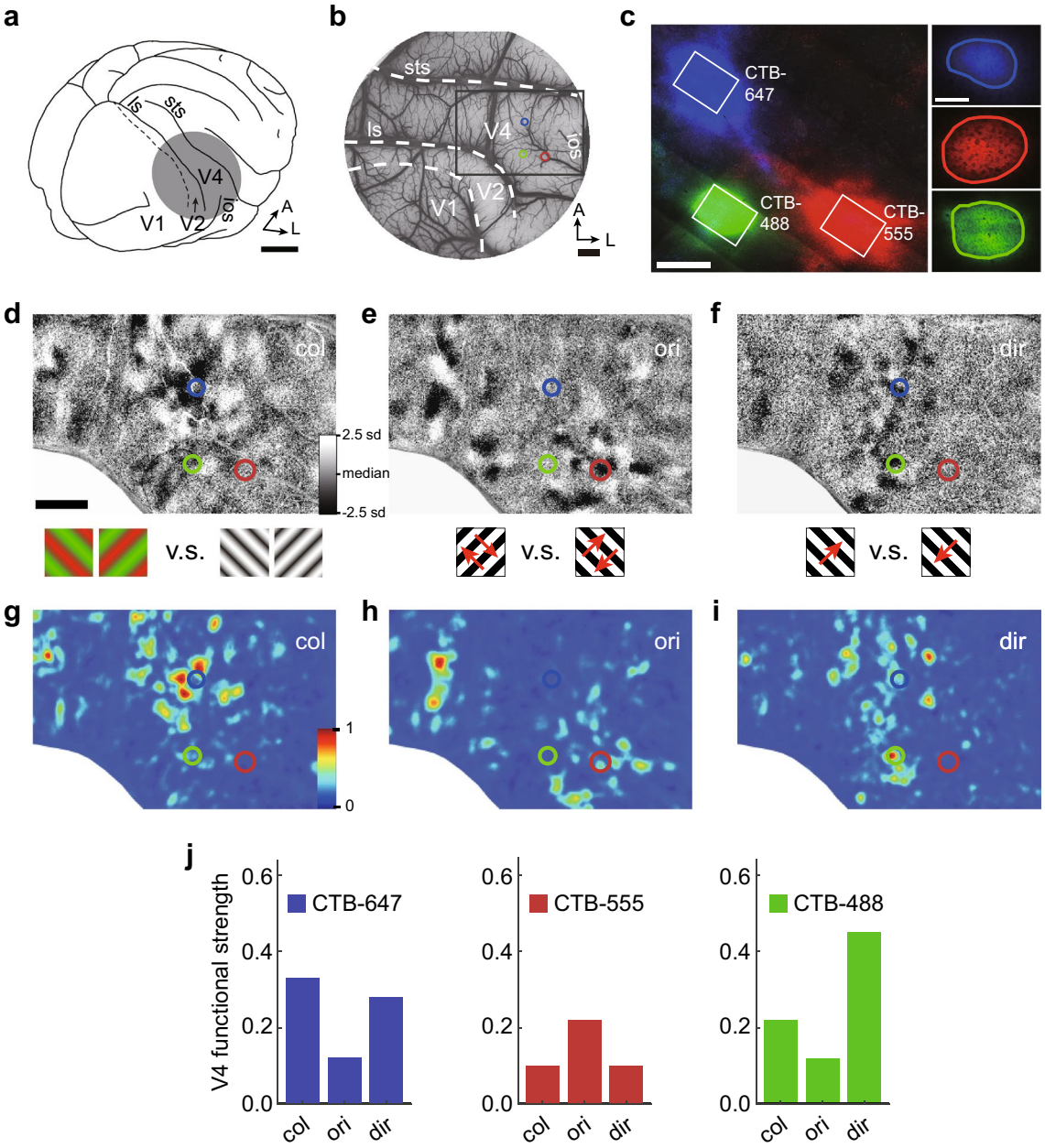

Fig. 1 V4 functional imaging and tracer injection sites in monkey A. **a** An illustration of a macaque brain and the imaging chamber location (shading). ls, lunate sulcus; sts, superior temporal sulcus; ios, inferior occipital sulcus; A, anterior; L, lateral. Scale bar: 10 mm. **b** Surface blood vessel pattern of the imaging chamber in monkey A. Circles represent tracer diffusion sizes (green: CTB-488; red: CTB-555; blue: CTB-647), measured from the tracer uptake zones in c. The black framed region is enlarged in d–i. Dashed lines represent area borders. Scale bar: 2 mm. **c** Left panel: Confocal fluorescence image of a V4 section showing the three injection sites. Scale bar: 1 mm. Right panels show the tracer uptake zones of the framed regions imaged from this or adjacent sections and from which the diameters of injection sites were measured. Scale bar: 0.3 mm. **d** Color versus luminance map of area V4 (black framed region in b) obtained by comparing cortical responses to color and luminance gratings (illustrated below). The map was clipped at the median ± 2.5 SD. The colored circles are the same as in b. Scale bar: 2 mm. **e** An orientation-preference map for the same region as in d. **f** A direction-preference map for the same region as in d. **g–i** Functional strength map for color (g), orientation (h), and direction (i) obtained based on the contrast maps shown above. Functional strengths were then measured as the average pixel values within the circles. **j** Normalized functional strength values for the three injection sites, each with three values, corresponding to the three functional maps

were used. The connection tube was filled with silicone oil, and the tracer was drawn into the glass pipette from its tip. A small amount of air (~40 nl) was drawn into the tip. Under a surgical microscope, the pipette was perpendicularly lowered to the planned V4 site based on the surface blood vessel pattern. The pipette tip was lowered into

Table 1 Case information

Case information		V4 information									V2 information		
Site	Anm.	Tracer	Depth (mm)	Vol. (nl)	Dia. (mm)	Section Method	Layers Involved*	V4 functional strength			Neuron number		
								Color	Ori.	Dir.	Thin	Pale	Thick
No. 01	A	CTB-488	1.40	30	0.61	Tangential	III, IV	0.22#	0.12	0.45#	12101	3547	1282
No. 02	A	CTB-555	1.30	30	0.72	Tangential	III, IV, V	0.10	0.22#	0.10	1728	3042	873
No. 03	A	CTB-647	1.30	30	0.59	Tangential	III, IV, V	0.33#	0.12	0.28#	2130	551	1570
No. 04	B	CTB-488	0.90	30	0.56	Tangential	III, IV	0.06	0.58#	0.15	1375	6404	2455
No. 05	B	CTB-555	1.10	30	0.83	Tangential	III, IV, V	0.21#	0.17	0.27#	1960	747	3319
No. 06	B	CTB-647	0.90	30	0.52	Tangential	III, IV	0.11	0.45#	0.14	746	1534	372
No. 07	C	CTB-647	0.65	100	0.87	Tangential	III, IV	0.31#	0.07	0.29#	12992	2596	1598
No. 08	D	CTB-488	1.10	35	0.62	Perp.	III, IV	0.06	0.24#	0.34#	2501	8259	8116
No. 09	D	CTB-555	1.00	35	0.51	Perp.	III, IV, V	0.40#	0.10	0.64#	5012	1458	1262

Anm. animal, *Vol.* volume, *Dia.* diameter, *Ori.* orientation, *Dir.* direction, *Perp.* perpendicular

*Layers involved by traction injections (tracer uptake zones can be discerned)

#Injection sites located close to functional domains (i.e., strength > 0.18)

the cortex to a depth of 0.65–1.40 mm (Table 1), and then tracer injection started. The pipette was withdrawn 0.1 mm after half the volume was injected, i.e., half of the volume was injected at the target depth, and the remaining half was injected after 0.1 mm withdrawal. The injection rate was 30 nl/min. The tracer volume (30–100 nl, see Table 1) was measured starting when the air disappeared from the visible tip. After the injection, the pipette was held in place for 10 min before retraction. One to three injections were administered to each animal (different tracers for different functional sites). An imaging chamber (Li et al. 2013; Tang et al. 2020) was implanted. In vivo fluorescence images (e.g., Fig. S1b-c) were examined immediately or 1 week after the tracer injections to confirm tracer loading and to determine the center of tracer diffusion. We used a Brucker Ultima IV Extended Reach microscope (Bruker Nano Inc.). The frame size was 654 × 540 pixels, covering 3.9 × 3.2 mm. For CTB-488, CTB-555, and CTB-647, we used 500–548 nm, 574–608 nm, and 663–735 nm emission filters, respectively. Images were montaged and aligned to the surface blood vessels (e.g., Fig. S1a–c).

Histology and areal delineation

Eighteen to 23 days after the tracer injection, the animals were killed with an overdose of sodium pentobarbital (80–100 mg/kg, i.v.) or thiopental sodium (125 mg/kg, i.v.) and perfused transcardially (step 1: 2 L of phosphate buffer saline, step 2: 1 L of phosphate buffer saline containing 2% paraformaldehyde, and step 3: 1 L of phosphate buffer saline containing 2% paraformaldehyde and 10% sucrose; all pH 7.4). The brain tissue containing the lunate sulcus was separated, and the lunate sulcus was flattened. The brain tissue containing the injection sites was separated without unfolding. The tissues were postfixed in phosphate buffer containing 2% paraformaldehyde and 30% sucrose at room temperature for 2–3 h. Then, the tissues were cryoprotected in 30% sucrose in phosphate buffer overnight at a temperature of 4 °C. The flattened tissues from all monkeys and tissues containing the injection sites from monkeys A–C were sectioned in the plane tangential to the cortical surface using a freezing microtome (Rem-710, Yamato). Several hole markers were created with a used microelectrode perpendicular to the surface (with ~ 5 mm intervals) to aid in subsequent coarse alignments of sections. The first section, which contained surface blood vessels, was sectioned at a thickness of 120–150 µm, and the remaining sections were 60–80 µm thick. For monkey D, the tissue containing injection sites was sectioned in the plane perpendicular to the cortical surface at an 80 µm thickness. Most of the sections were loaded onto a glass slide and sealed with cover glasses for fluorescence imaging. For monkeys A, B, C, and D, 3 (of 11), 3 (of 14), 1 (of 10), and 2 (of 11) flattened sections, respectively, were selected for CO staining (Wong-Riley 1979) and imaging (MVX10, Olympus, 1 × objective). The depths of the CO sections ranged from 0.45 to 1.10 mm, with a spacing of 0.16–0.24 mm. For monkeys A, B, and C, fluorescence imaged sections were Nissl stained and imaged using the same method as for CO staining. For monkey D, half of the perpendicularly sectioned sections were selected for Nissl staining.

For fluorescence imaging of sections, we used a confocal microscope (A1R, Nikon) and a 10 × objective. The structure of labeled neurons (soma) was determined by adjusting the software parameters (laser power, PMT amplification, and offset) to ensure that the labeled neuron sufficiently bright

but not overexposed. The software parameters were adjusted to a very low level to determine the tracer uptake zone. For CTB-488, CTB-555, and CTB-647, we used 500–550 nm, 570–620 nm, and 663–738 nm emission filters, respectively. These monochromatic channels were colored green, red, and blue, respectively, in the software (Nis-Elements). These three channels were then merged. In the merged images, neurons were identified manually based on their color and structure of the soma: red, green, or blue neurons indicate CTB-488, CTB-555, or CTB-647, respectively; yellow, cyan, or magenta neurons indicate double-labeled neurons. We did not include triple-labeled neurons (white) since some nonneuronal noise (blood vessels and dust) also appeared white. These triple-labeled neurons accounted for less than 1% of the total labeled neurons. Images of fluorescence labeling and CO staining in adjacent sections were aligned with zooming, rotation, and warping according to the radial blood vessels (imtransform, MATLAB, e.g., Fig. S1d–k). The ISOI maps, in vivo fluorescence maps, and images of the first section were aligned based on the surface blood vessel pattern (e.g., Fig. S1a–c). The center of the injection site was determined based on the in vivo fluorescence images (Fig. S1c). The diameters of the injection sites were determined from in vitro confocal fluorescence maps of sections (e.g., Fig. 1c and S2): for monkeys A–C, V4 tissues were sectioned in the plane tangential to the cortical surface. Tracer uptake zones were discerned where no labeled cell bodies were discernible (Federer et al. 2013). It has been shown that, besides the main target of layer 4, V2–V4 projections also terminates at layer 3 and deep layers, and usually form vertical columns (Rockland and Pandya 1979; Gattass et al. 1997). In this study, tracer uptake zones were mainly observed in layers 3 and 4, and in several cases in layer 5 (Table 1). Tracer injection sizes (diameters, Table 1) were measured from the section close to layer 4 and had the largest uptake zone. Finally, layer information was verified by performing Nissl staining of these sections (Fig. S2a, b). For monkey D, V4 tissue was sectioned in the plane perpendicular to the surface, and layers were detected using Nissl staining (Fig. S2d). The diameters of tracer uptake zones were determined according to the largest dense core in layer 3 and 4 from the section that had the largest core diameter.

The CO stripes were determined by overlaying two to three images of serial CO sections without obvious impairment, aligning the radial blood vessels, and merging the images (mean) in MATLAB. Thin and thick CO stripes were identified based on the width of the densely stained stripes and their alternating patterns in CO cycles. All seven authors performed the identification task independently and their results were compared. 48.6% of the thin or thick stripes exhibited greater than 86% consistency (i.e., at least 6 of 7 authors agreed). These stripes were labeled with uppercase letters (N, K) and the rest of the stripes were labeled with lowercase letters (n, k) in the CO images (e.g., Fig. 2b). In one case (monkey C), we also obtained three functional strength maps (color, orientation, and direction) from area V2 and aligned these maps to CO sections to facilitate the CO classification (Fig. S5). The CO-stained sections were no longer suitable for fluorescence imaging. The numbers of labeled neurons in these sections were estimated based on the average numbers of labeled neurons in their neighboring sections to obtain an accurate cell count.

Data analysis

Functional maps

V4 functional maps (e.g., Fig. 1d–f) were obtained with established support vector machine (SVM) methods (Xiao et al. 2008; Chen et al. 2016). Compared with regular subtraction maps, SVM maps have a better signal/noise ratio while maintaining the linear relationship of the map signals. For each stimulus condition, we first obtained a baseline subtracted image using the following formula: $dR/R = (R_{6\text{-}14} - R_{1\text{-}3})/R_{1\text{-}3}$, in which $R_{6\text{-}14}$ is the average of frames 6–14 and $R_{1\text{-}3}$ is the average of frames 1–3 (frames 1–2 (prestimulus frames) and frame 3 (frame imaged immediately after the stimulus onset that exhibits very low visual responses)). Two sets of dR/R images (e.g., from color and luminance stimuli) were then used to train an SVM classifier (LIBSVM, Chang and Lin 2011). An optimal classifier was obtained after fivefold cross-validation. The weight map of the trained SVM classifier was used as the functional map (e.g., Fig. 1d–f), in which a pixel value represents the contribution of the pixel to the classification. Each map was bandpass filtered (high cutoff: 0.2 mm/cycle, average 6 pixels/cycle, low cutoff: 3 mm/cycle).

Functional strength of the injection site

For area V4 in each case, we obtained one color map (color vs. luminance), two orientation maps (0° vs. 90° and 45° vs. 135°), and four direction maps (0° vs. 180°, 45° vs. 225°, 90° vs. 270°, and 135° vs. 315°). A color strength map was created with the absolute values of the color map pixels. Similarly, an orientation strength map was created by combining the absolute values of the two orientation maps using the mean value of each pixel. A direction strength map was obtained from the four direction maps with the same method. Each of the three functional strength maps was then normalized to 0–1 (Fig. 1g–i). The mean pixel values of the three functional strength maps within injection cores (e.g., circles in Fig. 1g–i) were then used as the functional strength values of the V4 injection sites in the subsequent data analysis.

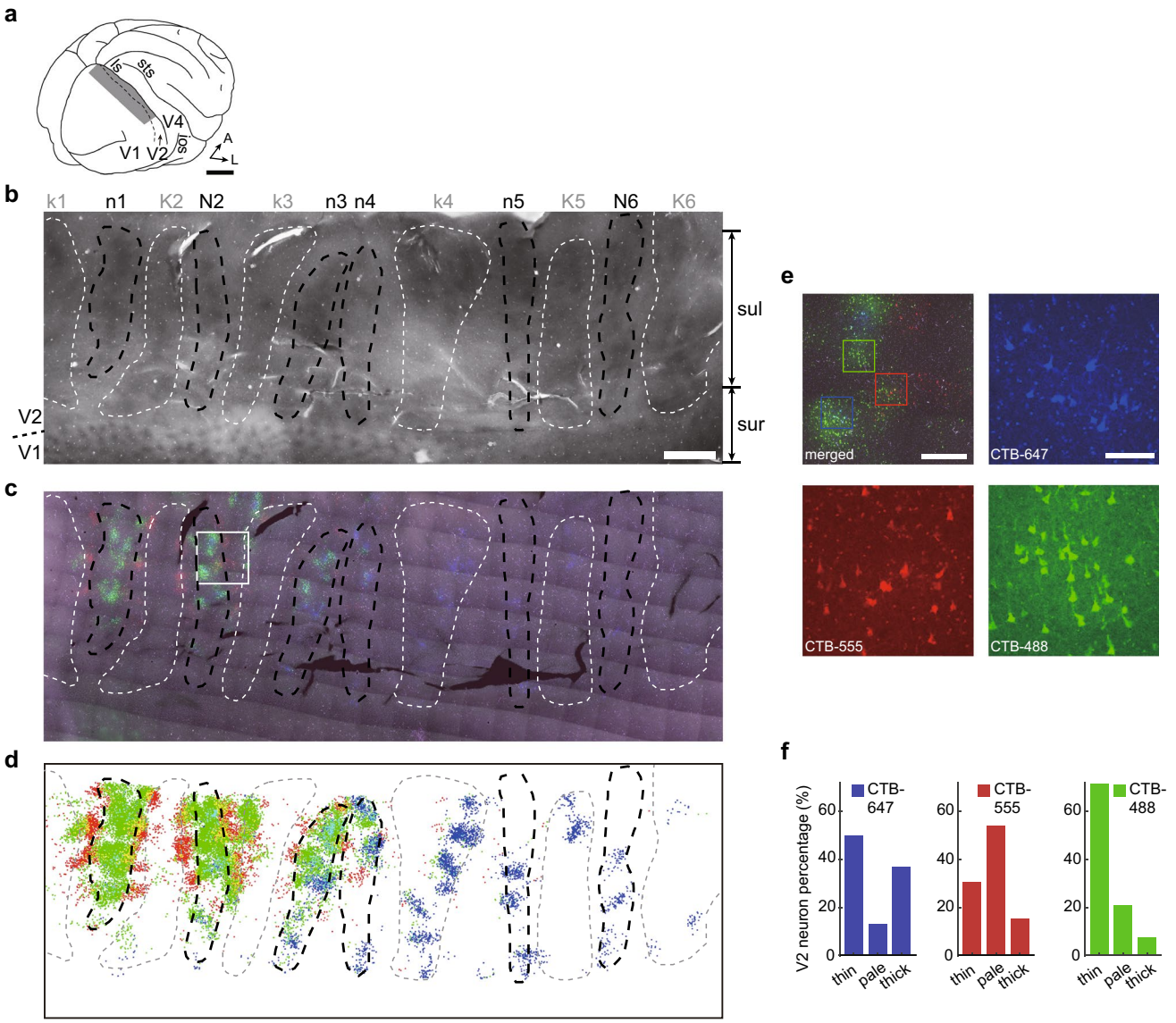

Fig. 2 Retrogradely labeled neurons in V2 CO stripes in monkey A. **a** Illustration of a macaque brain and regions of V2 (shading). Scale bar: 10 mm. **b** Average image of two sections stained with CO. Thin and thick stripes are labeled with corresponding letters. Uppercase letters ('N' or 'K') are used for stripes identified with higher certainty (see Methods). Lowercase letters ('n' or 'k') are used for stripes identified with less certainty. sul, area buried in the sulcus; sur, area exposed on surface. Scale bar: 2 mm. **c** A fluorescence image of a single V2 section that was aligned to the CO image shown above. The white framed region is shown at higher magnification in e. **d** All labeled neurons overlaid on CO stripe outlines. Labeled neurons are represented by colored dots. Colors for neuron overlap regions were merged. **e** Top left panel: a high magnification view of the framed region in c, scale bar: 0.5 mm. The other three panels are single-wavelength images of the corresponding framed regions of the same color in the top left panel (note that the color of these 3 images was added off-line and does not represent imaging light wavelengths). Scale bar: 0.1 mm. **f** Distributions of labeled neurons in three types of CO stripes for each tracer in monkey A. For comparisons among tracers, neuron numbers were normalized in each tracer and plotted as percentages

Correlation analysis and linear regression

For each tracer, percentages of the labeled neurons were calculated for each stripe type (the numerator was the number of neurons in one stripe type, and the denominator was the number of neurons in all three types of stripes). Spearman's correlation coefficients (corr, MATLAB) were calculated between V4 functional strength values and percentages of V2-labeled neurons (Fig. 4a–i), as well as between V4 functional strength values (Fig. 5) to investigate the potential connection patterns between V2 CO stripes and V4 functional domains. A linear regression (polyfit, MATLAB) was also calculated for each of these pairs. The

goodness of fit was evaluated with the following formula: $R^2 = 1 - \sum_{k=1}^{n} \left(y_k - \hat{y}_k\right)^2 / \sum_{n=1}^{n} \left(y_k - \overline{y}\right)^2$, in which y_k ($k = 1, 2\ldots$, n, n represents the number of data points) are the original data values and $\overline{y}$ is the average of these values. $\hat{y}_k$ ($n = 1, 2\ldots$, n) represents the values from the regression curve.

Results

Four hemispheres from four macaques were analyzed in this study. For each hemisphere, color, orientation, and motion direction maps in area V4 were first obtained from anesthetized animals using ISOI (Li et al. 2013). V4 sites with different functional properties were selected and used for tracer injection.

Functional properties of the V4 injection sites

Figure 1a–c shows the V4 injection sites in monkey A. This monkey received 3 injections, all of which were close to the foveal representation of V4. Figure 1d–f shows contrast maps obtained by comparing V4 responses to different visual stimuli. Black and white pixels in these maps represent regions preferentially activated by the stimuli illustrated on the left or right, respectively. Figure 1g–i shows the corresponding strength maps for the functional maps described above. Each map was obtained by calculating the mean absolute values of a type of contrast map(s) and then normalizing them (see Methods). For each injection, we obtained three functional strength values (color, orientation, and direction) from the corresponding strength maps by calculating the mean pixel values inside the largest injection uptake zones (circles in Fig. 1g–i). The sizes of the tracer uptake zones were determined based on in vitro fluorescence imaging of the tracer cores (Fig. 1c right panel). The centers of the injections were carefully determined in in vivo fluorescence images (Fig. S1a–c). The three injection sites had different response properties (Fig. 1j): site 1 (blue, CTB-647) exhibited strong responses to both color and direction, site 2 (red, CTB-555) mainly responded to orientation, and site 3 (green, CTB-488) mainly responded to direction and color. Next, we examined whether these differences caused systematic changes in labeled neurons in V2.

Retrogradely labeled neurons in V2

Figure 2b shows the CO staining results in V2 of monkey A (the same monkey shown in Fig. 1). Thick (K) and thin (N) stripes were determined based on their width and the alternating order. Lowercase letters (n, k) indicate where the identification of stripes is less certain (see Method). Confocal fluorescence images show clear V2 neurons labeled with different tracers (Fig. 2c, e). In Fig. 2d, colored dots represent all labeled neurons from multiple examined sections. For each color (tracer), the labeled neurons formed several bands perpendicular to the V1/V2 border. CTB-488 (green)- and CTB-555 (red)-labeled neurons appear to be mainly located in thin and pale stripes, respectively. CTB-647 (blue)-labeled neurons are found in both thin and thick stripes, but we also notice that the stripe types here are less certain (n4, k4, and n5). Note that CTB-555 (red)- and CTB-488 (green)-labeled neurons occupy neighboring regions, but have little overlap (yellow, mainly in thin pale borders). For each tracer, we calculated the distribution of its labeled neurons among the three stripe types (Fig. 2f). We compared distributions across different tracers and cases by calculating percentages of neurons for each tracer instead of neuron numbers (see the Methods). CTB-647 was injected into a V4 region close to the color and direction domains (Fig. 1j, left panel), and its labeled neurons in V2 were mainly located in thin and thick stripes (Fig. 2f, left panel). CTB-555 was close to a V4 orientation domain (Fig. 1j, middle panel), and its V2 labeled neurons were mostly found in pale stripes (Fig. 2f, middle panel). For CTB-488, the V4 injection site was close to the direction and color domains (Fig. 1j, right panel), and its labeled neurons in V2 were mostly located in thin stripes (Fig. 2f, right panel). Thus, certain correlations appeared between the V4 injection sites (and their functional properties) and the distribution of labeled neurons in V2.

Figure 3 shows a second example case (monkey D) in which two tracers were injected (Fig. 3a, b). CTB-555 was injected into a V4 site with strong color and direction selectivity, and the labeled V2 neurons were mainly found in thin stripes (red dots, Fig. 3e). CTB-488 was injected into a V4 site with strong orientation and direction selectivity, and its labeled neurons were mainly detected in pale stripes. Note that the overlapping regions (yellow, mainly located at thin pale borders) were very small, indicating a high degree of parallel projection. Other tracer injections showed similar trends (Fig. S3-S5). This qualitative observation is examined quantitatively below. We performed nine injections in four hemispheres from four monkeys. Detailed information on the injection sites and labeled neurons in V2 is shown in Table 1.

V2-V4 correlation analysis

We analyzed the relationship between the functional strengths of the V4 injections and the distributions of labeled neurons in V2 CO stripes by constructing scatter plots of these two factors (Fig. 4a-i). Each plot comprises nine data points, representing nine tracer injections. For each injection, the *X* axis value represents its functional strength in one functional map, and the *Y* axis value represents its

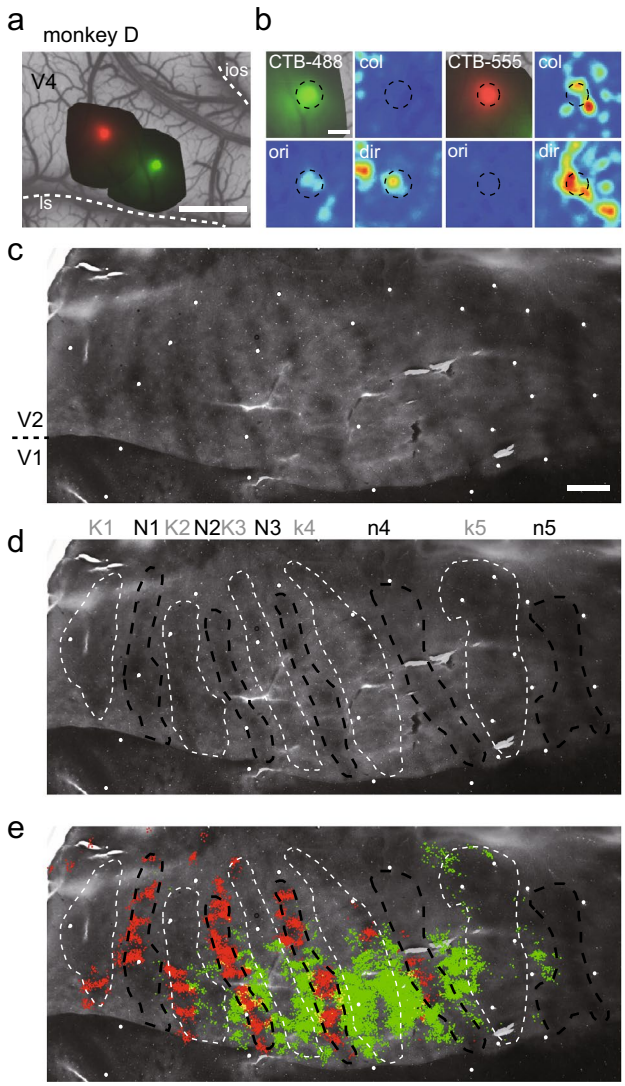

Fig. 3 The injection and projection results for monkey D. **a** In vivo fluorescence image of the tracer injections overlaid on a V4 surface blood vessel map. The centers of injection sites were determined according to the image. Scale bar: 2 mm. **b** Left panel: in vivo fluorescence image of CTB-488 and corresponding functional maps (col, color; ori, orientation; dir, direction). Dashed circles represent the tracer uptake zone determined in this study, as shown in Fig. S2e. Right panel: tracer CTB-555. Scale bar: 0.5 mm. **c** CO image of the examined V2 region, showing CO stripes oriented perpendicular to the V1/V2 border. Scale bar: 2 mm. **d** Same CO image as shown in c but with the stripes identified (same plot conventions as in Fig. 2b). **e** All labeled V2 neurons (dots) overlaid on the CO images (same as c, d). The colors are merged for neuron overlap regions

percentage of labeled V2 neurons in a certain stripe type. The dotted line represents the linear regression of these data points.

As shown in Fig. 4a, the percentages of labeled neurons in thin stripes were positively correlated (Fig. 4j) with the color strengths of the V4 injection sites. Namely, when the injection site was closer to the center of the V4 color domains, more labeled neurons were observed in the V2 thin stripes. This positive correlation was not present in V2 pale—V4 color (negative correlation in Fig. 4b) or V2 thick—V4 color (correlation close to zero in Fig. 4c) plots. In addition, neurons projecting to the V4 color domains tended to be located close to the center of the thin stripes (Fig. S7b, e). Taken together, these results indicated that V4 color modules tended to receive inputs from V2 thin stripes.

The V4 orientation feature positively correlated with the V2 pale stripe, indicating a contribution from the V2 pale stripes to the V4 orientation domains (Fig. 4e). V2 thin stripes, in contrast, appeared to avoid projecting to V4 orientation (negative correlation in Fig. 4d). The correlation between the thick stripe and orientation feature was close to zero (Fig. 4f). Thus, neurons projecting to the V4 color and orientation domains had very different distribution patterns in V2 stripes (also see Fig. S7).

Figure 4g shows that the V4 direction domain positively correlated with the V2 thin stripes. A possible explanation for this finding is that many of the direction domains we selected for injection also displayed strong color responses (see Fig. 5 and Discussion). As shown in Fig. 4h, i, the V4 direction had negative or zero correlations with pale and thick stripes, respectively, indicating that the V4 direction domains did not tend to receive input from V2 pale or thick stripes. Since V2 direction neurons were more likely to be located in thick stripes, V4 direction domains are unlikely to be a main projection target for V2 motion direction-selective neurons. For each plot, Spearman's correlation coefficient and the slope of linear regression were calculated and are illustrated in Fig. 4j, k.

The slopes of the nine plots in Fig. 4a–i are related to each other. One reason is that the functional maps in V4 have certain spatial correlations. For example, the color and orientation domains in V4 tend to occupy complementary regions (Tanigawa et al. 2010; Li et al. 2013). We analyzed functional maps in 13 V4 cases, including 4 cases in this study and 9 additional cases. Two-dimensional plots of the color response and orientation responses in V4 showed a negative relationship, thus confirming the previous findings (Fig. 5a). In addition, the selection of tracer injection sites is also important. In this study, the color and orientation properties of the nine injection sites also showed a negative correlation (Fig. 5f, i), consistent with the map features. In Fig. 4, the slopes in the first and second rows are opposite to each other, which may reflect this negative relationship. In contrast, the V4 direction domain was positively correlated with the V4 color (Fig. 5b) and orientation domain (Fig. 5c), consistent with previous findings (Li et al. 2013). The color and orientation properties of the 9 injection sites showed positive and negative correlations with direction, respectively (Fig. 5g–i). Another factor that affects the independence of the scatter plot slopes is that

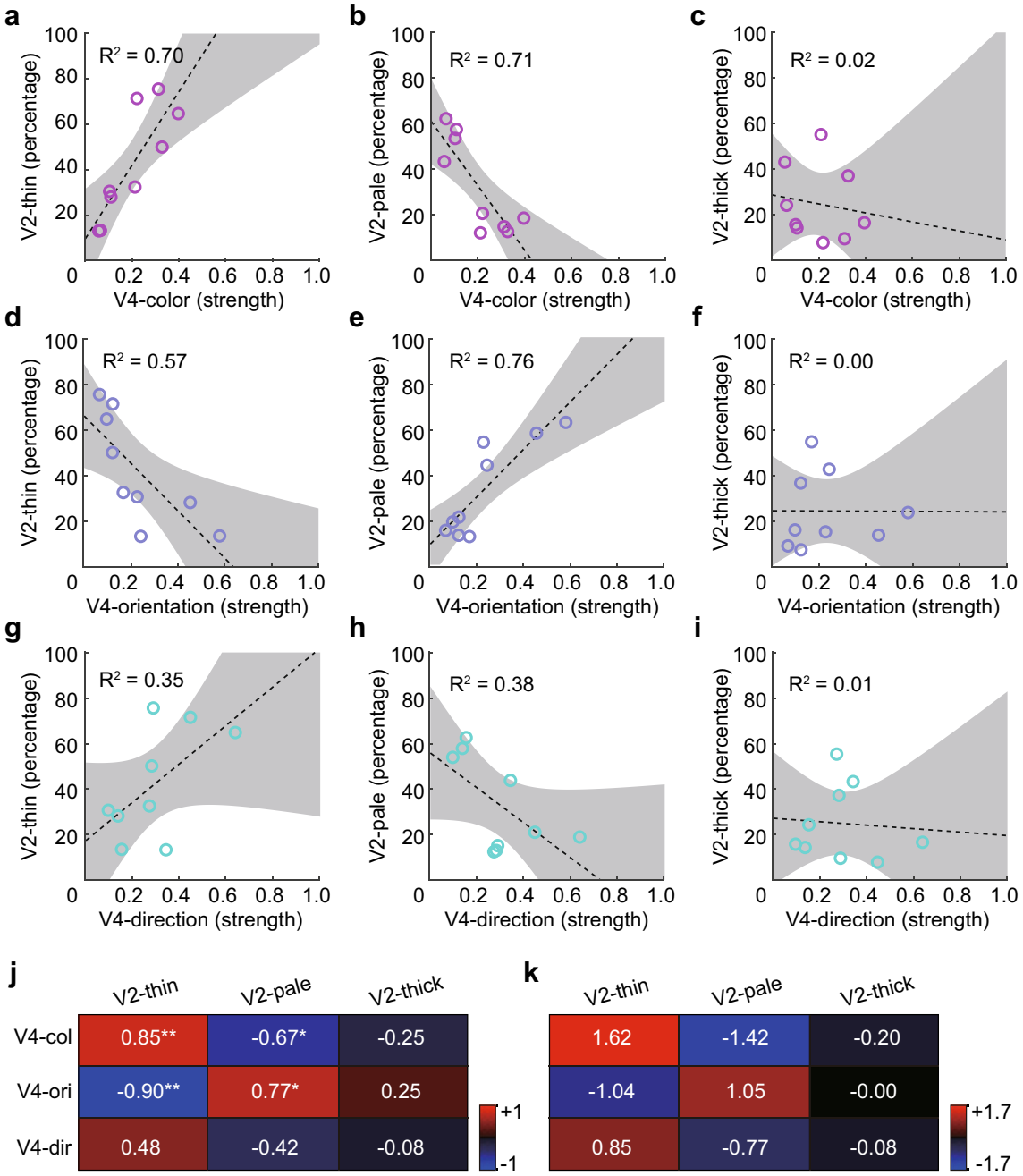

Fig. 4 Correlations between V4 injection sites and V2-labeled neurons. **a-i** Scatter plot of injection site properties (functional strengths, *X* axis) and labeled neuron properties (percentages, *Y* axis) for all nine injections (9 open circles) in four monkeys. Dotted lines represent linear regression of the data points, and gray regions represent 95% confidence intervals. **j** Spearman's correlation coefficients for the nine plots shown above. Asterisks indicate that the correlation is significantly different from zero (*$p < 0.05$, **$p < 0.01$, ***$p < 0.001$). **k** Slope values of the regression lines in the nine plots shown above

V2 neuron numbers were normalized within a tracer group (to percentages). Since the percentages of three stripes add up to 100%, increasing the percentage of one stripe always causes the other 1 or 2 percentages to decrease. Thus, for three plots in a row, their slopes would not have the same sign (i.e., all positive or all negative). Normally, a weak positive slope or a zero slope may become negative because of this factor. Finally, V4 functional maps were individually normalized (e.g., Fig. 1g–i). Based on an examination of their original subtraction maps (d*R*/*R* values), orientation and color maps had similar strengths (0.39‰ and 0.43‰, respectively), whereas direction maps

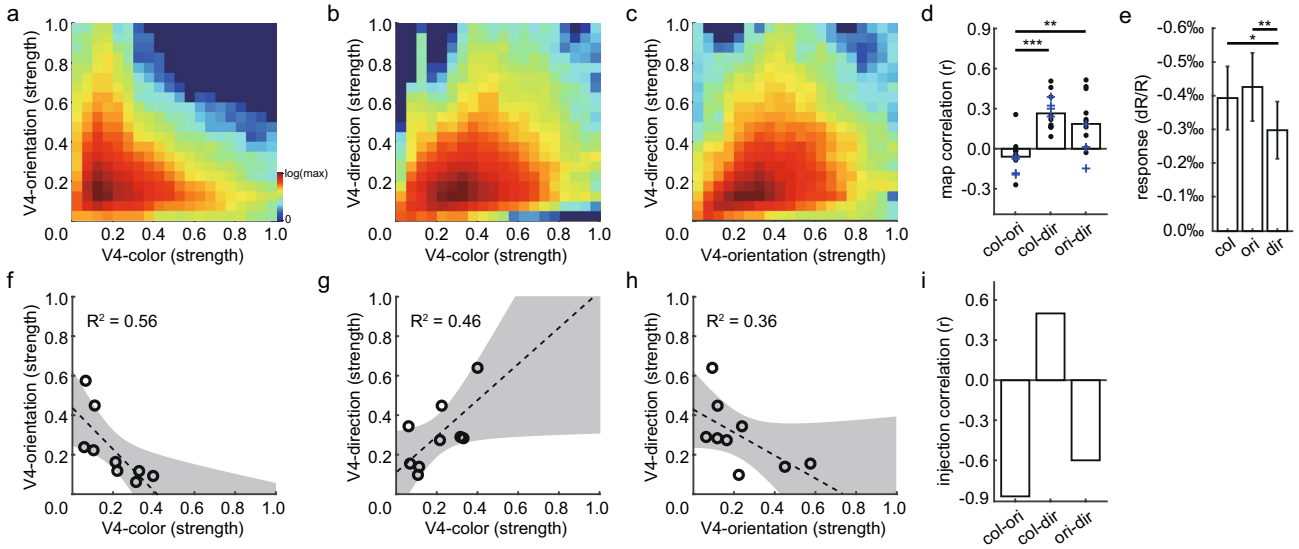

Fig. 5 Correlated functional properties of the maps and injection sites. **a** Pixel density map showing pixel numbers with a certain color strength (*X* axis) and orientation strength (*Y* axis). This map shows the average of data from 13 cases. The color and orientation strengths were calculated using the same approach as described in Fig. 1g-h. Strong color-selective pixels normally have weak orientation selectivity and vice versa. **b** Similar to a, but for direction and color strengths. Strong direction-selective pixels tended to have a strong color selectivity. **c** Similar to a but for direction and orientation strengths. Strong direction-selective pixels tended to have a strong orientation selectivity. **d** Spearman's correlation coefficients for map pairs in a-c. Every cross or dot represents one case. Blue crosses are for monkeys A, B, C, and D. $*p<0.05$; $**p<0.01$; $***p<0.001$, *t test*. **e** Average response magnitudes (dR/R) of color, orientation, and direction maps. The results were obtained from the same cases as in d. Error bar, SD. **f–h** Scatter plots of different injection site properties for all nine injections (9 open circles). **i** Spearman's correlation coefficients for scatter plots in f–h

had a relatively weaker map strength (0.29‰, Fig. 5e). Therefore, the correlations we observed for the V4 direction feature were more easily affected by the other two factors (color and orientation).

In this case, the strong positive correlation ($r>0$) in Fig. 4 was explained as the existence of a corresponding V2–V4 connection. A negative correlation ($r<0$) or near zero correlation ($r\approx 0$) was normally explained as an absence of a corresponding V2–V4 connection after considering multiple factors, including the spatial relationships between functional maps in V4 (Fig. 5a–d), the properties of V4 injection sites (Fig. 5f–i), and the normalization procedure for V2 neuron numbers.

Figure 6 summarizes our findings. Among V2–V4 projections, V2 thin stripes mainly project to V4 color modules (Fig. 4a). V2 pale stripes mainly project to V4 orientation modules (Fig. 4e), and V2 thick stripes send fewer projections to V4 than the other two stripes and have the weakest correlations with V4 functional domains (Fig. 4c, 4f, and 4i). Pale and thick stripes do not project to V4 direction modules (Fig. 4h–i). We did not clearly determine whether thin stripes project to V4 direction modules (Fig. 4g, also see "Discussion").

Discussion

In this study, we injected retrograde tracers into different functional modules in V4 and examined the patterns of labeled neurons in V2. We observed functionally specific projections from V2 CO stripes to V4 functional modules. In this study, functional and projection factors were quantified to determine the correlation between these two factors. The results not only confirmed previous anatomical findings, but also established a relationship between V2 CO stripes and V4 functional modules.

Parallel visual processing

The existence of functional modules, as well as the parallel projections among these modules, indicates that the processing of visual information occurs in parallel. In V2–V4 projections, previous studies revealed that thin and pale stripes project to different regions in V4, whereas thick stripes rarely project to V4 (De Yoe and Van Essen 1985; Zeki and Shipp 1989). The same projection patterns were also observed in New World monkeys (Nascimento-Silva et al. 2003, 2014). Our findings are generally consistent with these earlier findings. The additional information we provide is the functional properties of these V4 targets. Our findings

generally support the hypothesis that visual features are processed in parallel in the visual pathway.

However, increasing evidence has also shown that different visual features (color, form, motion, and depth) are not processed strictly in parallel. A large degree of integration has been observed at both the single-cell and functional architecture levels. First, multidimensional neurons were observed at all levels of visual processes. For example, many V2 neurons exhibit dual selectivity for color and orientation (Gegenfurtner et al. 1996; Shipp et al. 2009; Peres et al. 2018). Second, functional modules are not pure. In V2, orientation and direction neurons are also detected in thin stripes, and color neurons are found in pale and thick stripes (Gegenfurtner 2003; Peres et al. 2018). Third, different types of functional modules often exhibit different levels of overlap (e.g., Fig. 5a–d).

Taken together, the processing of visual features in early- to mid-tier visual cortices is neither pure parallel nor pure integrative. The overall picture appears to be partially mixed visual features are processed in partially overlapped functional modules and are relayed in parallel to the (partially overlapped) functional modules in the next stage. Additionally, the same types of information (e.g., orientation) processed in different functional modules (e.g., pale and thick stripes) are eventually sent to different downstream areas (e.g., V4 or MT). The functional significance of this processing strategy is worth further investigation, and new techniques such as high-density recording probes and two-photon imaging may contribute to answering this question.

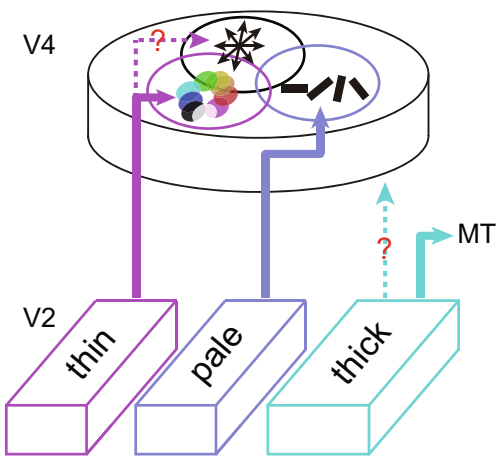

Fig. 6 Summary of functional inputs to V4 from V2. In V2–V4 projections, V4 color domains mainly receive inputs from V2 thin stripes (Fig. 4a), whereas V4 orientation domains mainly receive inputs from V2 pale stripes (Fig. 4e). Although we have not yet clearly determined whether V4 direction domains receive inputs from V2 thin stripes (Fig. 4g), they do not systematically receive inputs from thick or pale stripes (Fig. 4h-i). Some weak and unbiased projections from thick stripes to V4 may be due to uncertainty in identifying stripe types based on CO images

Labeled neurons in thick stripes

Previous studies have reported a lack of V2 thick stripe projections to V4 (DeYoe and Van Essen 1985; Shipp and Zeki 1985; Nascimento-Silva et al. 2003). Our results show certain thick stripe V4 projections. We discuss here the possible technical reasons for this discrepancy. First, some degree of uncertainty in identifying CO stripes existed. Since thin and pale stripes both project to V4, misclassifying CO stripes will increase the percentage of labeled thick neurons. We found that many labeled thick neurons were in "less certain" thick stripes (e.g., stripe k4 in Fig. 2d). In all certain and less certain CO stripes, the labeled thick neurons account for 24.6% of the total labeled neurons. If only those "certain" thick stripes were counted, this proportion decreased to 18.8%. Thus, our relatively high percentage of labeled thick neurons may be due to uncertainty in stripe identification. We subsequently repeated the correlation analysis based on "certain" CO stripes (Fig. S6) and found that the correlation trends were the same. Therefore, the main conclusions of the correlation still hold. Second, the identification of borders between thick and pale stripes has some uncertainty. Previous studies also identified some V4-projecting thick neurons. Examples are shown in Fig. 1c (middle panel) in the study by Nakamura et al. (1993) and Fig. 5 in the study by Zeki and Shipp 1989. These neurons were mainly located at the edge of thick stripes or patches of thick regions with weaker CO intensity. V2 projections to area MT are related to CO-dense patches within thick stripes (Shipp and Zeki 1989). Thus, the weak CO regions in thick stripes might alternatively project to V4. Regardless of these conjectures, our results show that thick projections to V4 had no obviously preferred targets. Its correlations and slopes to V4 functional domains were all close to zero (Fig. 4c, f, i).

Taken together, the projection from thick stripes to V4, if it exists, is minor. The actual strength of this projection should be less than what has been observed due to the uncertainty in the CO stripe identification.

Origin of V4 direction selectivity

Thus far, we have obtained a relatively clear map of the information sources for V4 color and orientation features. However, the inputs to V4 that carry direction-selective motion information remain unclear. Many (13–33%) V4 neurons have direction selectivity (Desimone and Schein 1987; Ferrera et al. 1994a), some of which cluster into direction domains (Li et al. 2013). One potential region that provides input is V2, where direction neurons are mostly located in thick stripes. However, our results show

that V4 direction domains do not receive inputs from V2 thick or pale stripes (Fig. 4h, i). In addition, our preliminary imaging results also show that V4 direction domains do not receive inputs from V2 direction domains (Fig. S5j). Thus, V4 direction domains are unlikely to obtain their motion inputs from V2 thick or pale stripes. Regarding the positive correlation between the V4 direction and V2 thin stripes (Fig. 4g), one possibility is that a major input to the V4 direction domain is V2 thin stripes. This possibility is less likely but not unreasonable, since direction neurons are present in V2 thin stripes, although fewer of these neurons are present in this location than in thick stripes (Peterhans and von der Heydt 1993; Gegenfurtner et al. 1996; Peres et al. 2018). Another more likely possibility is that the phenomenon that V4 direction domains receive inputs from V2 thin stripes is a by-product of the positive correlation between V2 thin stripes and the V4 color domain, because the V4 injection sites we selected generally exhibited positively correlated color and direction strengths (Fig. 5g), and V4 color neurons (not direction neurons) received inputs from V2 thin stripe projections. Compared with the V4 color domains, the clustering of the V4 direction domains was weaker (inferred from map strengths, see Fig. 5e), and the tracing results were more likely dominated by the connection patterns of color neurons. Indeed, a weaker V4 direction domain to V2 thin stripe correlation (0.48, Fig. 4g, j) is observed compared with the V4 color domain to V2 thin stripe correlation (0.85, Fig. 4a, j). Finally, a V1 lesion study (Schmid et al. 2013) also suggests that V4 direction selectivity may not depend on V1-related sources (including V2). If this hypothesis is true (V4 direction domains do not receive inputs from V2 thin stripes), then V2 is unlikely the source of V4 direction selectivity. More differences in color and direction selectivity in our injection sites to differentiate their inputs are needed to prove this hypothesis.

Another potential source for V4 direction selectivity is area MT, since direct projections from MT to V4 have been identified (Maunsell and van Essen 1983; Ungerleider et al. 2008). However, previous studies selectively inhibited magnocellular (M) or parvocellular (P) layers in the lateral geniculate nucleus (LGN) and found that V4 direction selectivity does not particularly rely on M or P input (Ferrera et al. 1992, 1994b). This finding is different from what was observed in MT neurons, whose response mainly relied on M inputs (Maunsell et al. 1990). Thus far, no evidence has shown that V4 direction neurons obtain direction selectivity from the MT.

Since V4 receives inputs from many other visual areas (Ungerleider et al. 2008), all are potential sources for V4 direction selectivity. One study has shown that after V1 lesion, the response of V4 direction neurons is relatively better preserved than that of other types of V4 neurons (Schmid et al. 2013). Thus, V4 direction-selective neurons may mainly rely on subcortical inputs that bypass V1. In summary, V4 direction neurons do not seem to rely on inputs from V1, V2, or MT and form a spatialized group in V4 visual processing.

In addition to color, orientation, and direction, V4 has other functional architectures, such as size (Ghose and Ts'o 1997), curvature (Hu et al. 2020; Tang et al. 2020), binocular disparity (Tanabe et al. 2005; Fang et al. 2019), border ownership (Franken and Reynolds 2021), and solid shape (Srinath et al. 2021). The functional inputs from V2 responsible for these V4 functional architectures can be studied using a similar approach.

Supplementary Information The online version contains supplementary material available at https://doi.org/10.1007/s00429-021-02440-3.

Acknowledgements This work was supported by the National Natural Science Foundation of China (31625012, 31530029, and 31371111). We thank Dr. Xiaohui Zhang and Dr. Yousheng Shu for their valuable technical support. We thank laboratory members (Rendong Tang, Heng Ma, Qianling Song, Pengcheng Li, Jie Lu, Yan Xiao, Peichao Li, Jiaming Hu, Haoran Xu, and Yang Fang) for providing technical assistance.

Author contributions CF, KY, CL, JW, RZ and XC performed the experiments; CF, HDL and KY designed the research; all the authors participated in the analysis; CF and HDL interpreted the results and wrote the paper. All authors read and approved the final manuscript.

Funding The work was supported by National Natural Science Foundation of China (Grant numbers: 31625012, 31530029, and 31371111).

Availability of data and material All data have been included in the manuscript and supporting information. Original data are available upon reasonable request.

Code availability Codes are available upon reasonable request.

Declarations

Conflict of interest The authors have no conflicts of interest to declare.

Ethical approval All procedures were performed in accordance with the National Institutes of Health Guidelines and were approved by the Institutional Animal Care and Use Committee of Beijing Normal University.

Consent to participate Not applicable. No human subjects.

Consent for publication Not applicable. No human subjects.

References

Chang C-C, Lin C-J (2011) LIBSVM: a library for support vector machines. ACM Trans Intell Syst Technol TIST 2:1–27. https://doi.org/10.1145/1961189.1961199

Chen G, Lu HD, Roe AW (2008) A map for horizontal disparity in monkey V2. Neuron 58:442–450. https://doi.org/10.1016/j.neuron.2008.02.032

Chen M, Li P, Zhu S et al (2016) An orientation map for motion boundaries in macaque V2. Cereb Cortex 26:279–287. https://doi.org/10.1093/cercor/bhu235

Conway BR, Moeller S, Tsao DY (2007) Specialized color modules in macaque extrastriate cortex. Neuron 56:560–573. https://doi.org/10.1016/j.neuron.2007.10.008

De Yoe EA, Van Essen DC (1985) Segregation of efferent connections and receptive field properties in visual area V2 of the macaque. Nature 317:58–61. https://doi.org/10.1038/317058a0

De Yoe EA, Felleman DJ, Van Essen DC, McClendon E (1994) Multiple processing streams in occipitotemporal visual cortex. Nature 371:151–154. https://doi.org/10.1038/371151a0

Desimone R, Schein SJ (1987) Visual properties of neurons in area V4 of the macaque: sensitivity to stimulus form. J Neurophysiol 57:835–868. https://doi.org/10.1152/jn.1987.57.3.835

Fang Y, Chen M, Xu H et al (2019) An orientation map for disparity-defined edges in area V4. Cereb Cortex 29:666–679. https://doi.org/10.1093/cercor/bhx348

Federer F, Williams D, Ichida JM et al (2013) Two projection streams from macaque V1 to the pale cytochrome oxidase stripes of V2. J Neurosci 33:11530–11539. https://doi.org/10.1523/JNEUROSCI.5053-12.2013

Felleman DJ, Xiao Y, McClendon E (1997) Modular organization of occipito-temporal pathways: cortical connections between visual area 4 and visual area 2 and posterior inferotemporal ventral area in macaque monkeys. J Neurosci 17:3185–3200. https://doi.org/10.1523/JNEUROSCI.17-09-03185.1997

Ferrera VP, Nealey TA, Maunsell JH (1992) Mixed parvocellular and magnocellular geniculate signals in visual area V4. Nature 358:756–758. https://doi.org/10.1038/358756a0

Ferrera V, Rudolph K, Maunsell J (1994a) Responses of neurons in the parietal and temporal visual pathways during a motion task. J Neurosci 14:6171–6186. https://doi.org/10.1523/JNEUROSCI.14-10-06171.1994

Ferrera VP, Nealey TA, Maunsell JH (1994b) Responses in macaque visual area V4 following inactivation of the parvocellular and magnocellular LGN pathways. J Neurosci 14:2080–2088. https://doi.org/10.1523/JNEUROSCI.14-04-02080.1994

Franken TP, Reynolds JH (2021) Columnar processing of border ownership in primate visual cortex. bioRxiv. https://doi.org/10.1101/2021.08.06.455427

Gattass R, Sousa AP, Mishkin M, Ungerleider LG (1997) Cortical projections of area V2 in the macaque. Cereb Cortex 7:110–129. https://doi.org/10.1093/cercor/7.2.110

Gegenfurtner KR (2003) Cortical mechanisms of colour vision. Nat Rev Neurosci 4:563–572. https://doi.org/10.1038/nrn1138

Gegenfurtner KR, Kiper DC, Fenstemaker SB (1996) Processing of color, form, and motion in macaque area V2. Vis Neurosci 13:161–172. https://doi.org/10.1017/s0952523800007203

Ghose GM, Ts'o DY (1997) Form processing modules in primate area V4. J Neurophysiol 77:2191–2196. https://doi.org/10.1152/jn.1997.77.4.2191

Hu JM, Song XM, Wang Q, Roe AW (2020) Curvature domains in V4 of macaque monkey. Elife 9:e57261. https://doi.org/10.7554/eLife.57261

Hubel DH, Livingstone MS (1985) Complex–unoriented cells in a subregion of primate area 18. Nature 315:325–327. https://doi.org/10.1038/315325a0

Hubel DH, Livingstone MS (1987) Segregation of form, color, and stereopsis in primate area 18. J Neurosci 7:3378–3415. https://doi.org/10.1523/JNEUROSCI.07-11-03378.1987

Levitt JB, Kiper DC, Movshon JA (1994) Receptive fields and functional architecture of macaque V2. J Neurophysiol 71:2517–2542. https://doi.org/10.1152/jn.1994.71.6.2517

Li P, Zhu S, Chen M et al (2013) A Motion Direction Preference Map in Monkey V4. Neuron 78:376–388. https://doi.org/10.1016/j.neuron.2013.02.024

Lu HD, Chen G, Tanigawa H, Roe AW (2010) A motion direction map in macaque V2. Neuron 68:1002–1013. https://doi.org/10.1016/j.neuron.2010.11.020

Maunsell JH, van Essen DC (1983) The connections of the middle temporal visual area (MT) and their relationship to a cortical hierarchy in the macaque monkey. J Neurosci 3:2563–2586. https://doi.org/10.1523/JNEUROSCI.03-12-02563.1983

Maunsell JH, Nealey TA, DePriest DD (1990) Magnocellular and parvocellular contributions to responses in the middle temporal visual area (MT) of the macaque monkey. J Neurosci 10:3323–3334. https://doi.org/10.1523/JNEUROSCI.10-10-03323.1990

Nakamura H, Gattass R, Desimone R, Ungerleider LG (1993) The modular organization of projections from areas V1 and V2 to areas V4 and TEO in macaques. J Neurosci 12:3681–3691. https://doi.org/10.1523/JNEUROSCI.13-09-03681.1993

Nascimento-Silva S, Gattass R, Fiorani M Jr, Sousa APB (2003) Three streams of visual information processing in V2 of Cebus monkey. J Comp Neurol 466:104–118. https://doi.org/10.1002/cne.10878

Nascimento-Silva S, Pinõn C, Soares JGM, Gattass R (2014) Feedforward and feedback connections and their relation to the cytox modules of V2 in Cebus monkeys. J Comp Neurol 522:3091–3105. https://doi.org/10.1002/cne.23571

Pasupathy A, Popovkina DV, Kim T (2020) Visual functions of primate area V4. Annu Rev vis Sci 6:363–385. https://doi.org/10.1146/annurev-vision-030320-041306

Peres R, Soares JGM, Lima B et al (2018) Neuronal response properties across cytochrome oxidase stripes in primate V2. J Comp Neurol 527:651–667. https://doi.org/10.1002/cne.24518

Peterhans E, von der Heydt R (1993) Functional organization of area V2 in the alert macaque. Eur J Neurosci 5:509–524. https://doi.org/10.1111/j.1460-9568.1993.tb00517.x

Rockland KS, Pandya DN (1979) Laminar origins and terminations of cortical connections of the occipital lobe in the rhesus monkey. Brain Res 179:3–20. https://doi.org/10.1016/0006-8993(79)90485-2

Roe AW, Ts'o DY (1995) Visual topography in primate V2: multiple representation across functional stripes. J Neurosci 15:3689–3715. https://doi.org/10.1523/JNEUROSCI.15-05-03689.1995

Roe AW, Chelazzi L, Connor CE et al (2012) Toward a unified theory of visual area V4. Neuron 74:12–29. https://doi.org/10.1016/j.neuron.2012.03.011

Schmid MC, Schmiedt JT, Peters AJ et al (2013) Motion-sensitive responses in visual area V4 in the absence of primary visual cortex. J Neurosci 33:18740–18745. https://doi.org/10.1523/JNEUROSCI.3923-13.2013

Shipp S, Zeki S (1985) Segregation of pathways leading from area V2 to areas V4 and V5 of macaque monkey visual cortex. Nature 315:322–324. https://doi.org/10.1038/315322a0

Shipp S, Zeki S (1989) The organization of connections between areas V5 and V2 in macaque monkey visual cortex. Eur J Neurosci 1:333–354. https://doi.org/10.1111/j.1460-9568.1989.tb00799.x

Shipp S, Zeki S (2002) The functional organization of area V2, I: specialization across stripes and layers. Vis Neurosci 19:187–210. https://doi.org/10.1017/S0952523802191164

Shipp S, Adams DL, Moutoussis K, Zeki S (2009) Feature binding in the feedback layers of area V2. Cereb Cortex 19:2230–2239. https://doi.org/10.1093/cercor/bhn243

Srinath R, Emonds A, Wang Q et al (2021) Early emergence of solid shape coding in natural and deep network vision. Curr Biol 31:51-65.e5. https://doi.org/10.1016/j.cub.2020.09.076

Tanabe S, Doi T, Umeda K, Fujita I (2005) Disparity-tuning characteristics of neuronal responses to dynamic random-dot stereograms in macaque visual area V4. J Neurophysiol 94:2683–2699. https://doi.org/10.1152/jn.00319.2005

Tang R, Song Q, Li Y et al (2020) Curvature-processing domains in primate V4. Elife 9:e57502. https://doi.org/10.7554/eLife.57502

Tanigawa H, Lu HD, Roe AW (2010) Functional organization for color and orientation in macaque V4. Nat Neurosci 13:1542–1548. https://doi.org/10.1038/nn.2676

Tso DY, Frostig RD, Lieke EE, Grinvald A (1990) Functional organization of primate visual cortex revealed by high resolution optical imaging. Science 249:417–420. https://doi.org/10.1126/science.2165630

Ts'o DY, Roe AW, Gilbert CD (2001) A hierarchy of the functional organization for color, form and disparity in primate visual area V2. Vision Res 41:1333–1349. https://doi.org/10.1016/S0042-6989(01)00076-1

Ungerleider LG, Galkin TW, Desimone R, Gattass R (2008) Cortical connections of area V4 in the macaque. Cereb Cortex 18:477–499. https://doi.org/10.1093/cercor/bhm061

Wang YI, Xiao Y, Felleman DJ (2007) V2 thin stripes contain spatially organized representations of achromatic luminance change. Cereb Cortex 17:116–129. https://doi.org/10.1093/cercor/bhj131

Wong-Riley M (1979) Changes in the visual system of monocularly sutured or enucleated cats demonstrable with cytochrome oxidase histochemistry. Brain Res 171:11–28. https://doi.org/10.1016/0006-8993(79)90728-5

Xiao Y, Zych A, Felleman DJ (1999) Segregation and convergence of functionally defined V2 Thin stripe and interstripe compartment projections to area V4 of macaques. Cereb Cortex 9:792–804. https://doi.org/10.1093/cercor/9.8.792

Xiao Y, Wang Y, Felleman DJ (2003) A spatially organized representation of colour in macaque cortical area V2. Nature 421:535–539. https://doi.org/10.1038/nature01372

Xiao Y, Rao R, Cecchi G, Kaplan E (2008) Improved mapping of information distribution across the cortical surface with the support vector machine. Neural Netw 21:341–348. https://doi.org/10.1016/j.neunet.2007.12.022

Zeki S, Shipp S (1989) Modular connections between areas V2 and V4 of macaque monkey visual cortex. Eur J Neurosci 1:494–506. https://doi.org/10.1111/j.1460-9568.1989.tb00356.x

Terms and Conditions

Springer Nature journal content, brought to you courtesy of Springer Nature Customer Service Center GmbH (“Springer Nature”).
Springer Nature supports a reasonable amount of sharing of research papers by authors, subscribers and authorised users (“Users”), for small-scale personal, non-commercial use provided that all copyright, trade and service marks and other proprietary notices are maintained. By accessing, sharing, receiving or otherwise using the Springer Nature journal content you agree to these terms of use (“Terms”). For these purposes, Springer Nature considers academic use (by researchers and students) to be non-commercial.
These Terms are supplementary and will apply in addition to any applicable website terms and conditions, a relevant site licence or a personal subscription. These Terms will prevail over any conflict or ambiguity with regards to the relevant terms, a site licence or a personal subscription (to the extent of the conflict or ambiguity only). For Creative Commons-licensed articles, the terms of the Creative Commons license used will apply.
We collect and use personal data to provide access to the Springer Nature journal content. We may also use these personal data internally within ResearchGate and Springer Nature and as agreed share it, in an anonymised way, for purposes of tracking, analysis and reporting. We will not otherwise disclose your personal data outside the ResearchGate or the Springer Nature group of companies unless we have your permission as detailed in the Privacy Policy.
While Users may use the Springer Nature journal content for small scale, personal non-commercial use, it is important to note that Users may not:

1. use such content for the purpose of providing other users with access on a regular or large scale basis or as a means to circumvent access control;
2. use such content where to do so would be considered a criminal or statutory offence in any jurisdiction, or gives rise to civil liability, or is otherwise unlawful;
3. falsely or misleadingly imply or suggest endorsement, approval , sponsorship, or association unless explicitly agreed to by Springer Nature in writing;
4. use bots or other automated methods to access the content or redirect messages
5. override any security feature or exclusionary protocol; or
6. share the content in order to create substitute for Springer Nature products or services or a systematic database of Springer Nature journal content.

In line with the restriction against commercial use, Springer Nature does not permit the creation of a product or service that creates revenue, royalties, rent or income from our content or its inclusion as part of a paid for service or for other commercial gain. Springer Nature journal content cannot be used for inter-library loans and librarians may not upload Springer Nature journal content on a large scale into their, or any other, institutional repository.
These terms of use are reviewed regularly and may be amended at any time. Springer Nature is not obligated to publish any information or content on this website and may remove it or features or functionality at our sole discretion, at any time with or without notice. Springer Nature may revoke this licence to you at any time and remove access to any copies of the Springer Nature journal content which have been saved.
To the fullest extent permitted by law, Springer Nature makes no warranties, representations or guarantees to Users, either express or implied with respect to the Springer nature journal content and all parties disclaim and waive any implied warranties or warranties imposed by law, including merchantability or fitness for any particular purpose.
Please note that these rights do not automatically extend to content, data or other material published by Springer Nature that may be licensed from third parties.
If you would like to use or distribute our Springer Nature journal content to a wider audience or on a regular basis or in any other manner not expressly permitted by these Terms, please contact Springer Nature at

onlineservice@springernature.com